
Rethinking Continual Learning with Progressive Neural Collapse

Zheng Wang¹ Wanhao Yu² Li Yang² Sen Lin¹

¹Department of Computer Science at University of Houston

²Department of Computer Science at University of North Carolina at Charlotte
{zwang214, slin50}@cougarnet.uh.edu, {wyu6, lyang50}@charlotte.edu

Abstract

Continual Learning (CL) seeks to build an agent that can continuously learn a sequence of tasks, where a key challenge, namely Catastrophic Forgetting, persists due to the potential knowledge interference among different tasks. On the other hand, deep neural networks (DNNs) are shown to converge to a terminal state termed Neural Collapse during training, where all class prototypes geometrically form a static simplex equiangular tight frame (ETF). These maximally and equally separated class prototypes make the ETF an ideal target for model learning in CL to mitigate knowledge interference. Thus inspired, several studies have emerged very recently to leverage a fixed global ETF in CL, which however suffers from key drawbacks, such as *impracticability* and *limited performance*. To address these challenges and fully unlock the potential of ETF in CL, we propose **Progressive Neural Collapse (ProNC)**, a novel framework that completely removes the need of a fixed global ETF in CL. Specifically, ProNC progressively expands the ETF target in a principled way by adding new class prototypes as vertices for new tasks, ensuring maximal separability across all encountered classes with minimal shifts from the previous ETF. We next develop a new CL framework by plugging ProNC into commonly used CL algorithm designs, where distillation is further leveraged to balance between target shifting for old classes and target aligning for new classes. Extensive experiments show that our approach significantly outperforms related baselines while maintaining superior flexibility, simplicity, and efficiency.

1 Introduction

Continual Learning (CL) has gained significant attention in recent years, aiming to build an agent to mimic the extraordinary human abilities to learn different tasks in a lifelong manner. A central challenge here is *Catastrophic Forgetting*, i.e., deep neural networks (DNNs) exhibit a pronounced tendency to lose previously acquired knowledge when trained on new tasks [27]. Within the spectrum of CL scenarios, class-incremental learning (CIL) presents the most formidable setting [26], where the model must not only address the current task by differentiating intra-task classes but also retain the knowledge of prior tasks by distinguishing historical classes from newly introduced ones. Nevertheless, achieving this dual objective remains particularly challenging, as evidenced by the suboptimal performance of existing CL methodologies.

Recent studies (e.g., [30]) have identified a compelling empirical phenomenon in DNN training termed *Neural Collapse (NC)*. During the terminal phase of training—when the training error asymptotically approaches zero—the last-layer features of samples within the same class converge to their class-specific mean, while the means of all classes align with their corresponding classifier prototypes. These prototypes further collapse geometrically to form the vertices of a *Simplex Equiangular Tight Frame (ETF)*, a maximally symmetric and separable configuration. This phenomenon results in

four critical properties: (1) *Feature Collapse*: Features from samples within the same class converge to their class-specific mean, effectively eliminating within-class variability. (2) *ETF Geometric Alignment*: The class-specific means for all classes align with the vertices of an ETF. (3) *Classifier-Prototype Equivalence*: These class means further align with the weights of the linear classifier. (4) *Decision Simplification*: Predictions reduce to a nearest-class-mean rule, where test samples are assigned to the class whose feature mean is the closest.

A key idea emerging here is that the elegant NC properties of DNN training naturally characterize an ideal model for CL: All classes seen so far, including the old classes for old tasks and the new classes for the current task, will have nearly-zero within-class variability, and their corresponding class-means are equally and perfectly separated. Several studies [54, 10, 53] have recently emerged to leverage NC and predefine a fixed global ETF as the model training target in CL, which however suffer from significant limitations: 1) Setting the number of vertices in the predefined ETF requires the knowledge of total class number encountered during CL before learning the first task, which is clearly not practical. 2) When the total class number is very large, the distance between any two vertices in the predefined ETF will be very small. Pushing class means towards these closely located vertices will unnecessarily hinder class discrimination, especially in early stages of CL when the number of seen classes that the model has to discriminate among is much smaller and the distance between these class means is larger. 3) NC posits that ETFs emerge naturally from feature convergence during training. Predefining the ETF contradicts this emergent behavior, as random initialization of the ETF risks geometric misalignment between learned features and the imposed topology.

To handle these limitations, a key insight is that the number of vertices in the target ETF for model training should match the total number of classes seen so far to achieve maximal across-class separation anytime in CL. Thus inspired, instead of relying on a predefined ETF with critical design flaws, we seek to develop a novel approach that can appropriately adapt the ETF target for CL in order to fully unleash the potential of NC. To this end, our contributions can be summarized as follows:

1) *A principled approach for ETF expansion*. By rethinking the objective of CL in classification as facilitating progressive NC with a growing ETF after learning each new task, we propose a novel approach, namely ProNC, to dynamically adjust the target ETF during CL. Specifically, ProNC first extracts the initial ETF target that emerges from first task training, and then expands the ETF target by adding new class prototypes as vertices prior to new task learning, to ensure maximal separability across all encountered classes without causing dramatic shifts from the previous ETF. In principle, ProNC can be broadly applied in CL frameworks as a new type of feature regularization.

2) *A simple and flexible framework for CL based on ProNC*. We next develop a new CL framework by plugging ProNC into commonly used CL algorithm designs. In particular, building upon the standard cross-entropy loss for new task learning, we introduce two additional losses, i.e., the alignment loss and the distillation loss. The former seeks to push the learned class features towards the corresponding target ETF provided by ProNC, whereas the later follows a standard idea of knowledge distillation to mitigate feature shifts for old classes. Guided by the target ETF, a nearest-class-mean classifier will be used to replace the standard linear classifier. Such a CL framework is very simple, without introducing any new complex designs, and flexible, where different components such as distillation can be replaced by other advanced designs.

3) *Comprehensive experiments for performance evaluation*. We perform comprehensive experiments on multiple standard benchmarks for both class incremental learning and task incremental learning, to evaluate the effectiveness of our CL approach compared with related baseline approaches. It can be shown that our approach significantly outperforms the baselines especially on larger datasets and also enjoys much less forgetting, without introducing more computation costs. In particular, extensive ablation studies are conducted to justify the benefits of ProNC in terms of maximizing feature separation among different classes and minimizing feature shifts across CL.

2 Related Work

Continual Learning. In general, existing CL approaches can be divided into several categories.

1) *Regularization-based approaches* seek to regularize the change on model parameters that are important to previous tasks [56, 7]. For instance, EWC [17] penalized updating important weights characterized based on Fisher Information matrix. MAS [1] characterized the weight importance

based on the sensitivity of model updates if this weight is changed. [24] proposed an approach that recursively modified the gradient update to minimize forgetting. The Bayesian framework has also been substantially investigated to implicitly penalize the parameter changes [20, 29, 57].

2) *Memory-based approaches* store information for previous tasks, which have shown very strong performance and can be further divided into two categories, i.e, rehearsal-based and orthogonal-projection based approaches. Rehearsal-based approaches [33, 8, 35] store a subset of data for previous tasks and replay them together with current data for new task learning. Some studies focused on how to select and manage the replay data to achieve better performance and efficiency, such as the use of reservoir sampling [9], coreset-based memory selection [3, 41], and data compression [43]. Some other studies investigated how to utilize the replay data, such as imposing constraints on gradient update [8], combining with knowledge distillation [32, 5, 15, 12], contrastive learning based approaches [6, 47]. The use of generative data has also been explored in CL for rehearsal-based approaches [39]. Instead of storing data samples, orthogonal-projection based approaches [11, 44, 37, 23, 22] store gradient or basis information to reconstruct the input subspaces of old tasks, so as to modify the model parameters only along the direction orthogonal to these subspaces.

3) *Architecture-based approaches* freeze the important parameters for old tasks, train the remaining parameters to learn new tasks and expand the model if needed. Notably, PNN [36] preserved the weights for previous tasks and progressively expanded the network architecture to learn new tasks. LwF [21] split the model parameters into two parts, where task-shared parameters are used to extract common knowledge and task-specific parameters are expanded for new tasks. Some studies [55, 16, 51] combined the strategies of weight selection, model pruning and expansion.

4) *Pretrained-model based approaches* leverage the powerful pretrained models and seek to efficiently adapt the models to continuously learn new tasks. To enable lightweight finetuning of the pretrained models in CL, prompt-based approaches have gained much attention by constructing a pool of prompts, selecting and optimizing the appropriate prompts for each task [46, 45, 40]. Some studies focused on how to leverage the strong representation capability of pretrained models. For example, [58] proposed a simple CL baseline that directly leverages the prototype features of the pretrained models without any training on new tasks. [28] proposed a frozen random projection layer to capture the interactions among features.

Neural Collapse. The NC phenomenon during the terminal state of DNN training was first discovered in [30], which has further motivated a lot of studies on understanding NC. For example, NC has been investigated under different settings, e.g., imbalanced learning [52, 49], and also been applied in different domains, e.g., semantic segmentation [38, 50] and language models [48, 59]. Very recently, several studies have emerged to leverage NC to facilitate better CL algorithm designs. [53] first proposed to use a fixed global ETF target for feature-classifier alignment in few-shot CL with an ETF classifier, whereas [54] applied the same idea to more general CL setups. [10] further integrated this idea with contrastive learning based CL. However, as mentioned earlier, the reliance on a fixed global ETF suffers from critical drawbacks, which we aim to address in this work.

3 Preliminaries

Problem Setup. We consider a general CL setup where a sequence of tasks $\mathbb{T} = \{t\}_{t=1}^T$ arrives sequentially. Each task t is associated with a dataset $\mathbb{D}_t = \{(\mathbf{x}_{t,i}, y_{t,i})\}_{i=1}^{N_t}$ containing N_t input-label pairs. A fixed capacity model parameterized by θ will be trained to learn one task at a time. This work focuses on two widely studied settings: class-incremental learning (Class-IL) and task-incremental learning (Task-IL). In both settings, there is no overlap in class labels across tasks, ensuring $\mathbb{D}_t \cap \mathbb{D}_{t'} = \emptyset$ for any two distinct tasks $t \neq t'$. In Class-IL, the model does not have task specific information, requiring all data to be classified through a unified global classifier. In Task-IL, task-specific identifier is provided, enabling classification via dedicated task-level classifiers.

Neural Collapse. To formally characterize the NC phenomenon [30] emerged during terminal training phases of DNNs, it is necessary to first define the simplex ETF geometry.

Definition 1 (Simplex Equiangular Tight Frame). *A simplex equiangular tight frame (ETF) is a set of vectors $\{\mathbf{e}_k\}_{k=1}^K \in \mathbb{R}^d$ ($d \geq K - 1$) with the following properties. 1) **Equal Norm:** All vectors have identical ℓ_2 -norm, i.e., $\|\mathbf{e}_k\|_2 = 1, \forall k \in \{1, \dots, K\}$. 2) **Equiangularity:** The inner product between any two distinct vectors is minimal and constant, i.e., $\mathbf{e}_{k_1}^\top \mathbf{e}_{k_2} = -\frac{1}{K-1}, \forall k_1 \neq k_2$. Then, a*

simplex ETF can be constructed from an orthogonal basis $\mathbf{U} \in \mathbb{R}^{d \times K}$ (where $\mathbf{U}^\top \mathbf{U} = \mathbf{I}_K$) via:

$$\mathbf{E} = \sqrt{\frac{K}{K-1}} \mathbf{U} \left(\mathbf{I}_K - \frac{1}{K} \mathbf{1}_K \mathbf{1}_K^\top \right), \quad (1)$$

where $\mathbf{E} = [\mathbf{e}_1, \dots, \mathbf{e}_K]$ is the ETF matrix, \mathbf{I}_K is the identity matrix, and $\mathbf{1}_K$ is the all-ones vector.

The NC phenomenon can be then characterized by the following four properties [30]:

(NC1): The last-layer features of samples within the same class collapse to their within-class mean, resulting in vanishing intra-class variability: the covariance $\Sigma_W^{(k)} \rightarrow \mathbf{0}$, where $\Sigma_W^{(k)} = \text{Avg}_i \{ (\boldsymbol{\mu}_{k,i} - \boldsymbol{\mu}_k)(\boldsymbol{\mu}_{k,i} - \boldsymbol{\mu}_k)^\top \}$, $\boldsymbol{\mu}_{k,i}$ is the feature of sample i in class k , and $\boldsymbol{\mu}_k$ is the within-class feature mean of class k ;

(NC2): The centered class means $\{\hat{\boldsymbol{\mu}}_k\}$ align with a simplex ETF, where $\hat{\boldsymbol{\mu}}_k = (\boldsymbol{\mu}_k - \boldsymbol{\mu}_G) / \|\boldsymbol{\mu}_k - \boldsymbol{\mu}_G\|$ and the global mean $\boldsymbol{\mu}_G = \frac{1}{K} \sum_{k=1}^K \boldsymbol{\mu}_k$;

(NC3): The centered class means align with their corresponding classifier prototypes, i.e., $\hat{\boldsymbol{\mu}}_k = \mathbf{w}_k / \|\mathbf{w}_k\|$, $1 \leq k \leq K$, where \mathbf{w}_k is the class prototype of class k ;

(NC4): Under NC1–NC3, predictions reduce to a nearest-class-center rule, i.e., $\arg \max_k \langle \boldsymbol{\mu}, \mathbf{w}_k \rangle = \arg \min_k \|\boldsymbol{\mu} - \boldsymbol{\mu}_k\|$, where $\boldsymbol{\mu}$ is the last-layer feature of a sample for prediction.

4 Continual Learning with Progressive Neural Collapse

4.1 Progressive Neural Collapse

To completely remove the need of predefining a global fixed ETF as the feature learning target for CL, we next seek to answer the following two important questions: 1) *How should the base ETF target be initialized?* 2) *How should the ETF target be adapted during CL?*

1) ETF initialization after first task learning. Previous studies [54] randomly initialize the ETF target because a global ETF that matches the total class number in CL needs to be defined, which could lead to potential misalignment between the predefined ETF and learned features during task learning. Note that during the training of Task 1 in CL, models trained through standard supervised learning theoretically develop last-layer class feature means $\{\boldsymbol{\mu}_c\}_{c=1}^{K_1}$ that converge to a simplex ETF $\mathbf{E}^{d \times K_1}$, where $\boldsymbol{\mu}_c \in \mathbb{R}^d$ and K_1 is the number of classes in Task 1. Thus motivated, the initial ETF should be extracted from the first task training to address the misalignment, which leads to an ETF target that matches the number of classes in the first task.

However, in practice it is difficult to fully reach the asymptotic convergence regime of model training with zero training loss, such that the learned class feature means $\tilde{\mathbf{M}}_{K_1} = \{\tilde{\boldsymbol{\mu}}_c\}_{c=1}^{K_1}$ for Task 1 will not strictly satisfy the ETF properties, as also corroborated in our empirical observations. Here $\tilde{\boldsymbol{\mu}}_c$ is the empirical feature mean over samples within the class c . To handle this, a key step is to find the right ETF target that is closest to $\tilde{\mathbf{M}}_{K_1}$ after the training for Task 1 converges, i.e.,

$$\mathbf{E}^* = \arg \min_{\mathbf{E}} \|\tilde{\mathbf{M}}_{K_1} - \mathbf{E}\|_F^2. \quad (2)$$

Towards this end, based on Definition 1, we can have the following theorem that characterizes the nearest ETF after learning the first task:

Theorem 1. Let $\mathbf{U}' = \sqrt{\frac{K_1-1}{K_1}} \tilde{\mathbf{M}}_{K_1} \left(\mathbf{I}_{K_1} - \frac{1}{K_1} \mathbf{1}_{K_1} \mathbf{1}_{K_1}^\top \right)$ and the SVD of \mathbf{U}' is $\mathbf{W} \boldsymbol{\Sigma} \mathbf{V}^\top$. Then the ETF matrix \mathbf{E}^* in Equation (2) can be obtained as follows:

$$\mathbf{E}^* = \sqrt{\frac{K_1}{K_1-1}} \mathbf{W} \mathbf{V}^\top \left(\mathbf{I}_{K_1} - \frac{1}{K_1} \mathbf{1}_{K_1} \mathbf{1}_{K_1}^\top \right). \quad (3)$$

Given the learned class feature means $\tilde{\mathbf{M}}_{K_1}$, Theorem 1 immediately indicates a three-step procedure to construct the initial ETF target that aligns well with the task learning: 1) Construct \mathbf{U}' from $\tilde{\mathbf{M}}_{K_1}$, 2) Conduct SVD on \mathbf{U}' , 3) Construct \mathbf{E}^* based on Equation (3).

2) ETF expansion prior to new task learning. Given the initial ETF matrix $\mathbf{E}_1 = \mathbf{E}^*$ where the number of vertices matches the number of classes in Task 1, the next step is to progressively expand the ETF target as new classes come in with new tasks, in order to achieve two objectives: 1) the number of newly expanded vertices in the new ETF target will match the number of new classes in the new task; 2) the vertices in the new ETF target that match old classes will not significantly shift from their original positions in the old ETF target, so as to reduce catastrophic forgetting.

A key insight here is that the ETF matrix \mathbf{E} is indeed determined by the corresponding orthogonal basis \mathbf{U} as shown in Equation (1), and keeping the orthogonal basis unchanged when expanding the ETF will in principle reduce the shift from the old ETF. This motivates a novel ETF expansion strategy by expanding the constructing orthogonal basis, which includes two steps:

(Step a) Let K_t represent the total number of classes until any task t . When a new task $t \geq 2$ arrives with $K_t - K_{t-1}$ classes, the ETF target expansion will be triggered before learning task t , which seeks to obtain a new target \mathbf{E}_t with K_t vertices from the previous ETF target \mathbf{E}_{t-1} with K_{t-1} vertices. In particular, the original orthogonal basis $\mathbf{U}_{t-1} \in \mathbb{R}^{d \times K_{t-1}}$ of \mathbf{E}_{t-1} will be expanded to $\mathbf{U}_t \in \mathbb{R}^{d \times K_t}$ by appending $K_t - K_{t-1}$ new orthogonal vectors. These new vectors are generated via Gram-Schmidt orthogonalization against the existing K_{t-1} basis vectors in \mathbf{U}_{t-1} , ensuring that \mathbf{U}_t retains orthonormality across all K_t vectors.

(Step b) Substituting \mathbf{U}_t and K_t into Equation (1) will lead to an expanded ETF target with K_t vertices. This extended ETF serves as the predefined geometric configuration for feature learning in task t , maintaining uniform angular separation and maximal equiangularity among all seen classes.

4.2 A Continual Learning Framework based on Progressive Neural Collapse

In what follows, we seek to incorporate the idea of progressive neural collapse (ProNC) into commonly used CL algorithm designs, where the model will be trained to push the learned class features towards the progressively expanded ETF for each task during CL.

More specifically, we focus on the model training for tasks $t \geq 2$, whereas the first task learning follows a standard supervised learning procedure with widely used loss functions, e.g., cross-entropy loss \mathcal{L}_{ce} . For tasks $t \geq 2$, we first apply ProNC to generate a newly expanded ETF target \mathbf{E}_t before learning task t . The loss function design for model training will include three different loss terms, i.e., a **supervised term**, an **alignment term**, and a **distillation term**. The first supervised term follows standard loss designs in CL and leverages the cross-entropy loss to facilitate intra-task classification, while we introduce the other two loss terms below in detail.

1) Alignment with the ETF target. The alignment loss pushes the learned class features towards the ETF target $\mathbf{E}_t = [\mathbf{e}_{1,t}, \dots, \mathbf{e}_{K_t,t}]$, which characterizes the cosine similarity between the feature $\boldsymbol{\mu}_{k,i}$ for sample i in class k and the corresponding vertex $\mathbf{e}_{k,t}$ in the ETF \mathbf{E}_t for class k [52, 54]:

$$\mathcal{L}_{\text{align}}(\boldsymbol{\mu}_{k,i}^t, \mathbf{e}_{k,t}) = \frac{1}{2}(\mathbf{e}_{k,t}^\top \boldsymbol{\mu}_{k,i}^t - 1)^2. \quad (4)$$

Here $\boldsymbol{\mu}_{k,i}^t$ corresponds to the normalized feature extracted from the last layer of the current model when learning task t . A small $\mathcal{L}_{\text{align}}$ implies that the learned normalized feature for each sample aligns well the corresponding ETF vertex for the class that the sample belongs to, minimizing the intra-class variability while forcing different class feature means equally separated. This indeed provides a new type of feature regularization based on ETF, which can be widely adopted and is also very powerful as shown later in our experimental results.

2) Distillation to further reduce forgetting. While ProNC expands the ETF target without dramatically shifting from the old ETF, the vertices that map to old classes will inevitably change after ETF expansion due to geometric properties of ETF. To handle this and further reduce catastrophic forgetting, we next borrow the idea of knowledge distillation, which is a widely used technique in CL to reduce catastrophic forgetting [32, 15, 5, 54]. In particular, we consider a typical distillation loss which characterizes the cosine similarity between the normalized features, for the same data sample, from the current model and that from the model obtained after learning the previous task, to maintain the simplicity and flexibility of our framework:

$$\mathcal{L}_{\text{distill}}(\boldsymbol{\mu}_{k,i}^{(t-1)}, \boldsymbol{\mu}_{k,i}^{(t)}) = \frac{1}{2}((\boldsymbol{\mu}_{k,i}^{(t-1)})^\top \boldsymbol{\mu}_{k,i}^{(t)} - 1)^2. \quad (5)$$

Here $\boldsymbol{\mu}_{k,i}^{(t-1)}$ is the normalized last layer feature for the sample i in class k extracted from the learned model after task $t - 1$.

To best unlock the potential of ProNC, we also leverage the standard data replay in the CL framework: the replay data from previous tasks will be mixed together with the current data before the current task learning, such that each minibatch of data during model training will include both replay data and current data. Combining all three loss terms will lead to the final instance-loss function:

$$\mathcal{L} = \mathcal{L}_{ce} + \lambda_1 \cdot \mathcal{L}_{\text{align}} + \lambda_2 \cdot \mathcal{L}_{\text{distill}}, \quad (6)$$

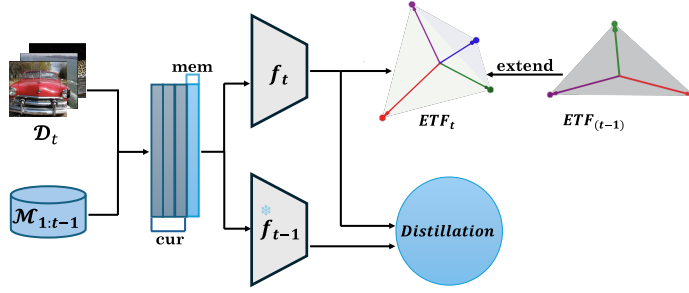


Figure 1: Overflow of our proposed CL framework for new task learning based on the mixture of current task data and replay data. The new model f_t is trained towards the expanded ETF target, with forgetting further reduced based on feature distillation.

which is averaged over all samples in a minibatch for model update. Here λ_1 and λ_2 are coefficients to balance between pushing the learned features towards the target ETF and reducing the vertex shift from the previous ETF for minimizing forgetting. The overall workflow is shown in Figure 1.

Inference. During inference for model performance evaluation, instead of using the linear classifier for classification, we leverage the widely used cosine similarity [31, 13, 42, 15] between the extracted sample feature from the learned model and the vertices in the target ETF as the classification criteria. Specifically, for any testing data sample i , let μ_j denote the normalized last layer feature extracted from the tested model. Then the class prediction result will be $\arg \max_k \mu_j^\top e_k$, where e_k is the k -th column vector in the target ETF.

5 Experimental Results

5.1 Experimental Setups

Datasets. We evaluate the performance on three standard CL benchmarks, i.e., **Seq-CIFAR-10** [18] that partitions 10 classes into 5 sequential tasks (2 classes per task), **Seq-CIFAR-100** [18] that comprises 10 tasks with 10 classes per task, and **Seq-TinyImageNet** [19] divides 200 classes into 10 sequential tasks (20 classes per task), and consider both Class-IL and Task-IL scenarios.

Baseline approaches. We evaluate our CL approach against state-of-the-art (SOTA) approaches, including various replay-based approaches, i.e., ER [34], iCaRL [32], GEM [25], GSS [2], DER [5], DER++ [5], and contrastive learning based approaches, i.e., Co²L [6], CILA [47], and MNC³L [10]. We also compare our approach with NCT [54] that predefines a fixed global ETF target.

Implementation details. To ensure a fair comparison, we train a ResNet-18 backbone [14] using the same number of epochs for all approaches, i.e., 50 epochs for every task in Seq-CIFAR-10 and Seq-CIFAR-100, where 100 epochs for every task in Seq-TinyImageNet to accommodate its higher complexity. For contrastive learning approaches Co²L, CILA, and MNC³L, we follow their original implementations by removing the final classification layer of ResNet-18, and append a two-layer projection head with ReLU activation to map backbone features into a d -dimensional embedding space ($d = 128$ for Seq-CIFAR-10/100, $d = 256$ for Seq-TinyImageNet). A separate linear classifier is subsequently trained on the frozen embeddings for these contrastive learning methods.

Evaluation metrics. We consider two standard evaluation metrics in CL [7, 5, 32, 10], i.e., final average accuracy (FAA) and average forgetting (FF). Let T denote the total number of tasks (start with task 0 and end with task $T - 1$) in CL and a_i^t be the model accuracy on the i -th task after learning the task $t \in [0, T - 1]$. The FAA and FF are defined as:

$$\text{FAA} = \frac{1}{T} \sum_{i=0}^{T-1} a_i^{T-1}, \quad \text{FF} = \frac{1}{T-1} \sum_{i=0}^{T-2} \max_{t \in \{0, \dots, T-2\}} a_i^t - a_i^{T-1}.$$

5.2 Main Results

Table 1 shows the performance comparison for both Class-IL and Task-IL under different memory budgets, i.e., buffer size 200 and 500. It is clear that our approach significantly and consistently outperforms all the baseline approaches across all considered CL settings, datasets, and buffer sizes. In particular, the performance improvement in our approach becomes more substantial on larger datasets and under a smaller buffer size. For example, consider a buffer size of 200. On Seq-CIFAR-

Table 1: Performance comparison under various setups. All results are averaged over multiple runs. The final version with error bars is in the appendix.

Buffer	Method	Seq-CIFAR-10		Seq-CIFAR-100		Seq-TinyImageNet	
		Class-IL	Task-IL	Class-IL	Task-IL	Class-IL	Task-IL
		FAA (FF)	FAA (FF)	FAA (FF)	FAA (FF)	FAA (FF)	FAA (FF)
200	ER [34]	44.79 (59.30)	91.19 (6.07)	21.78 (75.06)	60.19 (27.38)	8.49 (76.53)	38.17 (40.47)
	iCaRL [32]	49.02 (23.52)	88.99 (25.34)	28 (47.20)	51.43 (36.20)	7.53 (31.06)	28.19 (42.47)
	GEM [25]	25.54 (80.36)	90.44 (9.57)	20.75 (77.40)	58.84 (29.59)	—	—
	GSS [2]	39.07 (72.48)	88.8 (8.49)	19.42 (77.62)	55.38 (32.81)	—	—
	DER [5]	61.93 (35.79)	91.4 (6.08)	31.23 (62.72)	63.09 (25.98)	11.87 (64.83)	40.22 (40.43)
	DER++ [5]	64.88 (32.59)	91.92 (5.16)	28.13 (60.99)	66.80 (23.91)	11.34 (73.47)	43.06 (39.02)
	Co ² L [6]	51.27 (30.17)	84.69 (2.91)	18.09 (64.14)	49.19 (27.83)	12.95 (62.04)	38.40 (40.75)
	CILA [47]	59.68 (37.52)	91.36 (5.89)	19.49 (64.01)	53.93 (33.07)	12.98 (63.11)	37.32 (41.40)
	MNC ³ L [10]	51.09 (33.74)	85.07 (4.90)	15.81 (62.51)	43.91 (39.79)	10.57 (59.68)	32.78 (45.10)
	NCT [54]	51.59 (22.48)	80.63 (1.41)	26.38 (27.40)	75.75 (4.79)	10.95 (49.33)	52.71 (15.88)
	Ours	65.58 (32.75)	96.86 (0.65)	42.99 (36.07)	85.63 (4.40)	27.44 (42.81)	69.09 (9.42)
500	ER [34]	57.74 (43.22)	93.61 (3.50)	27.66 (67.96)	66.23 (17.37)	9.99 (75.21)	48.64 (30.73)
	iCaRL [32]	47.55 (28.20)	88.22 (22.61)	33.25 (40.99)	58.16 (27.90)	9.38 (37.30)	31.55 (39.44)
	GEM [25]	26.2 (78.93)	92.16 (5.60)	25.54 (71.34)	66.31 (20.44)	—	—
	GSS [2]	49.73 (59.18)	91.02 (6.37)	21.92 (74.12)	60.28 (26.57)	—	—
	DER [5]	70.51 (24.02)	93.40 (3.72)	41.36 (49.07)	71.73 (25.98)	17.75 (59.95)	51.78 (28.21)
	DER++ [5]	72.70 (22.38)	93.88 (4.66)	38.20 (49.18)	74.77 (15.75)	19.38 (58.75)	51.91 (25.47)
	Co ² L [6]	61.78 (17.79)	89.51 (2.65)	26.64 (48.60)	62.32 (23.47)	18.71 (49.64)	50.74 (13.80)
	CILA [47]	67.82 (18.22)	93.29 (0.65)	31.27 (45.67)	68.29 (16.98)	18.09 (64.14)	49.19 (27.83)
	MNC ³ L [10]	52.20 (27.88)	85.94 (3.15)	22.29 (46.09)	56.43 (24.29)	11.52 (44.96)	36.32 (39.00)
	NCT [54]	60.93 (13.82)	81.27 (3.84)	33.77 (27.85)	75.87 (5.06)	18.24 (50.90)	62.30 (6.84)
	Ours	73.95 (26.75)	96.95 (0.24)	48.94 (24.32)	86.38 (4.35)	29.06 (38.58)	69.77 (9.52)

100, our approach outperforms the best baseline approaches, i.e., DER for Class-IL and NCT for Task-IL, by 37.65% and 13.04%, respectively. On Seq-TinyImageNet, our approach outperforms the best baseline approaches, i.e., CILA for Class-IL and NCT for Task-IL, by 111.40% and 31.08%, respectively. In particular, the performance of our approach is outstanding when the buffer size is 200, especially for Task-IL when we focus on differentiating classes within a specific task. This implies that our approach is more robust to different buffer sizes and the principle of ProNC can even work well with a small amount of replay data. Moreover, by leveraging the NCT in a more principled manner, our approach dominates the previous approach NCT where a predefined global ETF target hinders class discrimination by unnecessarily forcing class means towards closely located vertices.

Besides, it can be seen from Table 1 that among most scenarios our approach and NCT achieve much less forgetting compared to other baseline approaches, while our approach shows even better forgetting than NCT in 8 out of 12 settings. The reason is because the vertices in the ETF target provide an fixed anchor and goal for old task features during new task learning, which the model training can follow much easily in the feature space. In other words, instead of simply constraining the shifts from old features or important weights as in previous studies, the ETF target offers an additional fixed goal from which the model should not shift the new features too far way. These results indicate the huge potential of leveraging NC and ETF in guiding the feature learning for CL.

More interestingly, in contrast to previous replay-based approaches [34, 32, 25, 2, 5] which require a replay buffer in principle, *our approach can even work without replay*. Specifically, with an *empty* replay buffer, our approach can achieve a FAA of 30.87% for Class-IL and 84.33% for Task-IL on Seq-CIFAR-100, and 24.43% for Class-IL and 68.08% for Task-IL on Seq-TinyImageNet, which almost outperforms all baselines in Table 1 under a buffer size of 200 and even of 500. *This phenomenal performance implies that our approach indeed offers a new and powerful feature regularization based on ProNC, which can be widely applied in various CL scenarios.*

5.3 Ablation Study

In what follows, we will conduct various ablation studies to build a comprehensive understanding of our approach, where most studies are for Class-IL on Seq-CIFAR-100 with a buffer size 500.

Feature learning behaviors. To understand the superior performance of our approach in contrast to important baseline approaches, we first delve into the feature learning behaviors during CL by characterizing different types of feature correlations. In particular, based on our analysis of the ETF target and Table 1, compared to NCT [54] with a predefined global ETF, our approach should enjoy the following benefits: 1) A lower cosine similarity between different class feature means which is also closer to theoretically maximum separation $-\frac{1}{K_t-1}$ for K_t seen classes until task t according to Definition 1.

This can be confirmed in Figure 2a, where we calculate $\text{Avg}_{k \neq k'} (\langle \frac{\mu_k - \mu_G}{\|\mu_k - \mu_G\|}, \frac{\mu_{k'} - \mu_G}{\|\mu_{k'} - \mu_G\|} \rangle + \frac{1}{K_t-1})$ of the features after learning every task t , averaged for any two seen classes k and k' . Thanks to ProNC,

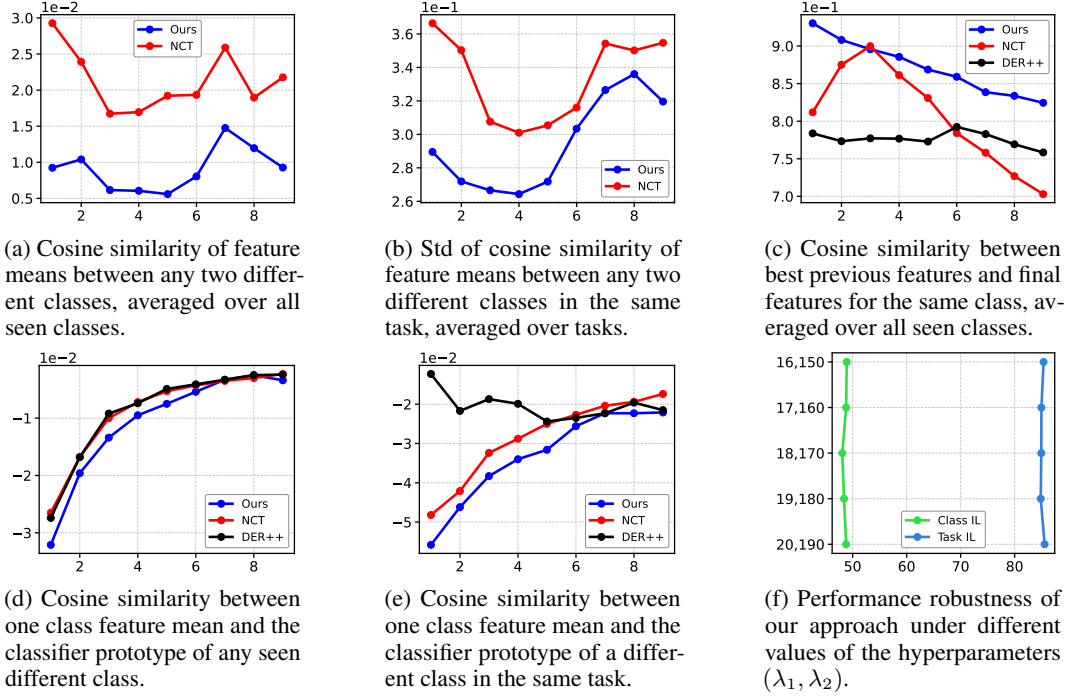


Figure 2: In (a)-(e), X-axis is the task ID during CL and Y-axis is the (average or std) value of the corresponding cosine similarity. In (f), X-axis is the accuracy FAA and Y-axis is the value of (λ_1, λ_2) .

our approach achieves a smaller value, which is also closer to 0, than NCT. 2) All class feature means should be almost equally separated within the same task. To show this, we evaluate the standard deviation (std) of across-class cosine similarity for the same task, averaged over all seen tasks in CL, i.e., $\text{Avg}(\text{std}(\langle \frac{\mu_k - \mu_G}{\|\mu_k - \mu_G\|}, \frac{\mu_{k'} - \mu_G}{\|\mu_{k'} - \mu_G\|} \rangle))$, where classes k and k' are in the same task. Figure 2b shows that our approach achieves a smaller average std (also closer to 0) than NCT, implying the different class means are closer to equal separation. Besides, we also follow the metrics in NCT [54] to evaluate 1) the cosine similarity between the feature mean of class k and the classifier prototype $w_{k'}$ of a different class k' , averaged over all seen classes until task t , and 2) the same cosine similarity but for classes within the same task which is averaged over all seen tasks during CL. As shown in Figure 2d and 2e, our approach achieves a lower cosine similarity compared to NCT and DER++, which implies easier class discrimination.

Moreover, Table 1 demonstrates the exceptional performance of our approach in addressing forgetting. To understand this, we characterize the cosine similarity between 1) the learned features from the best performing previous model and 2) that from the final model, for the same class, averaged over all seen classes so far. This is consistent to the definition of forgetting. As shown in Figure 2c, our approach achieves the higher similarity than both NCT and DER++, indicating its superior capability in handling feature shifts during CL and then minimizing forgetting based on ProNC.

Impacts of different components. To understand the impact of different design components on our approach, we investigate six different variants, as shown in Table 2. Here in (a)-(c) we remove one of the three loss terms in Equation (6), respectively. Clearly, removing either $\mathcal{L}_{\text{align}}$ or $\mathcal{L}_{\text{distill}}$ will significantly degrade the performance, highlighting the importance of the designed ETF target and the right balance between learning stability and plasticity. On the other hand, while removing \mathcal{L}_{ce} will slightly decrease the performance, this variant still outperforms the baseline approaches as shown in Table 1, indicating the benefit of our approach mainly from $\mathcal{L}_{\text{align}}$ and $\mathcal{L}_{\text{distill}}$. In (d), we predefine a base ETF target and expand it for new tasks based on ProNC, and the degraded performance shows the benefit of naturally aligning the base ETF with feature learning in the first task. In (e), we replace the entire ProNC with a predefined fixed global ETF as in [54] and the performance drops dramatically, corroborating the importance of ProNC for setting an appropriate ETF target in new task learning. In (f), we replace our cosine similarity based classifier by using

Table 2: Impact of different components.

Variant	Performance
Ours	48.94
(a) w/o \mathcal{L}_{ce}	44.97
(b) w/o $\mathcal{L}_{\text{align}}$	23.22
(c) w/o $\mathcal{L}_{\text{distill}}$	19.96
(d) w/ predefined base ETF	44.99
(e) w/ predefined global ETF	33.51
(f) w/ linear classifier	44.49

the standard linear classifier, and the performance drop further highlights the usefulness of ETF in classification by providing equally separated feature representation targets for different classes.

Training cost. To evaluate the computation efficiency of our approach, we summarize in Table 3 the average training time per epoch and per task for all approaches. It can be seen that our approach is more efficient than all considered replay-based approaches except iCaRL. The pronounced latency of GSS arises from its quadratic time complexity in gradient correlation computations ($O(N^2)$ under a buffer size N) and memory-intensive operations for maintaining sample importance matrices. In contrast, iCaRL achieves higher efficiency by employing a binary cross-entropy loss, which enjoy a constant time complexity per class ($O(1)$), compared to the linear class-dependent complexity ($O(C)$, C being the total number of classes) of conventional cross-entropy loss. Meanwhile, the per-epoch training time of our approach is comparable with the recent contrastive-learning based approaches. In summary, by leveraging NC in a principled way, our approach not only significantly outperforms baseline approaches by setting new SOTA performance, but also maintains a high efficiency due to the simplicity of our framework and robustness to buffer sizes. This highlights the great potential of our approach in practical resource-limited CL scenarios.

Table 3: Average training time per epoch and per task (seconds).

Method	Epoch	Task
ER [34]	3.03	151.48
iCaRL [32]	1.60	84.77
GEM [25]	3.26	162.64
GSS [2]	28.86	1425.26
DER [5]	3.07	153.21
DER++ [5]	5.03	253.34
Co ² L [6]	2.52	126.19
CIA [47]	2.77	138.59
MNC ³ L [10]	2.82	141.01
NCT [54]	3.41	172.02
Ours	2.91	146.71

More comparison with contrastive learning based approaches. Contrastive learning based approaches usually suffer from high computation costs due to the nature of contrastive learning with data augmentation. In the original implementation of these approaches, e.g., Co²L [6] and MNC³L [10], 500

Table 4: FAA, FF and total training time comparison with contrastive learning based approaches under their training setups.

Buffer	Method	Seq-CIFAR-100			Seq-TinyImageNet		
		Class-IL	Task-IL	Time(S)	Class-IL	Task-IL	Time(S)
200	Co ² L [6]	27.38 (67.82)	42.37 (38.22)	4362	13.88 (73.25)	42.37 (47.11)	12494
	MNC ³ L [10]	34.04 (52.40)	59.46(33.66)	3904	15.52 (52.07)	44.59 (33.76)	10922
	Ours	42.99 (36.07)	85.63 (4.40)	1482	27.44 (42.81)	69.09 (9.42)	12137
500	Co ² L [6]	37.02 (51.23)	62.44 (26.31)	4380	20.12 (65.15)	53.04 (39.22)	12100
	MNC ³ L [10]	40.25 (46.09)	65.85 (24.29)	3979	20.31 (46.08)	53.46 (26.45)	12669
	Ours	48.94 (24.32)	86.38 (4.35)	1588	29.06 (38.58)	69.77 (9.52)	12350

training epochs is used for the initial task, and followed by different epochs for each subsequent task, i.e., 100 epochs for Seq-CIFAR-100 and 50 epochs for Seq-TinyImageNet. To further demonstrate the superior performance of our approach, we evaluate our approach under the standard setup in this paper, i.e., 50 epochs for Seq-CIFAR-100 and 100 epochs for Seq-TinyImageNet, against these approaches under their original implementation in Table 4. Clearly, while the performance of the contrastive learning based approaches improves with more training epochs, our approach still achieves significantly better performance with an even shorter training time.

Robustness with respect to hyperparameters. We conduct experiments to demonstrate the impact of λ_1 and λ_2 in Equation (6). As shown in Figure 2f, the performance of our approach is very stable under a wide range of hyperparameter selections, indicating the robustness of our approach.

6 Conclusion

Neural collapse in DNN training characterizes an ideal feature learning target for CL with maximally and equally separated class prototypes through a simplex ETF, whereas recent studies leverage this by predefining a fixed global ETF target, suffering from impracticability and limited performance. To address this and unlock the potential of NC in CL, we propose a novel approach namely progressive neural collapse (ProNC), by initializing the ETF to align with first task leaning and progressively expanding the ETF for each new task without significantly shifting from the previous ETF. This will ensure maximal and equal separability across all encountered classes anytime during CL, without the global knowledge of total class numbers in CL. Building upon ProNC, we introduce a simple and flexible CL framework with minimal changes on standard CL frameworks, where the model is trained to push the learned sample features towards the corresponding ETF target and distillation with data replay is leveraged to further reduce forgetting. Extensive experiments have demonstrated the dominating performance of our approach against state-of-the-art baseline approaches, while maintaining superior efficiency and flexibility. One limitation here is that we assume clear task boundaries and it is interesting to see how our approach can be extended to more general setups. We hope this work will serve as initial steps for showcasing the great potentials of NC in facilitating better CL algorithm design and inspire further research in CL community along this interesting direction.

References

- [1] Rahaf Aljundi, Francesca Babiloni, Mohamed Elhoseiny, Marcus Rohrbach, and Tinne Tuytelaars. Memory aware synapses: Learning what (not) to forget. In *Proceedings of the European conference on computer vision (ECCV)*, pages 139–154, 2018.
- [2] Rahaf Aljundi, Min Lin, Baptiste Goujaud, and Yoshua Bengio. Gradient based sample selection for online continual learning. *Advances in neural information processing systems*, 32, 2019.
- [3] Zalán Borsos, Mojmir Mutny, and Andreas Krause. Coresets via bilevel optimization for continual learning and streaming. *Advances in neural information processing systems*, 33:14879–14890, 2020.
- [4] Matteo Boschini, Lorenzo Bonicelli, Pietro Buzzega, Angelo Porrello, and Simone Calderara. Class-incremental continual learning into the extended der-verse. *IEEE Transactions on Pattern Analysis and Machine Intelligence*, 2022.
- [5] Pietro Buzzega, Matteo Boschini, Angelo Porrello, Davide Abati, and Simone Calderara. Dark experience for general continual learning: a strong, simple baseline. *Advances in neural information processing systems*, 33:15920–15930, 2020.
- [6] Hyuntak Cha, Jaeho Lee, and Jinwoo Shin. Co²l: Contrastive continual learning. In *Proceedings of the IEEE/CVF International conference on computer vision*, pages 9516–9525, 2021.
- [7] Arslan Chaudhry, Puneet K Dokania, Thalaiyasingam Ajanthan, and Philip HS Torr. Riemannian walk for incremental learning: Understanding forgetting and intransigence. In *Proceedings of the European conference on computer vision (ECCV)*, pages 532–547, 2018.
- [8] Arslan Chaudhry, Marc’Aurelio Ranzato, Marcus Rohrbach, and Mohamed Elhoseiny. Efficient lifelong learning with a-gem. *arXiv preprint arXiv:1812.00420*, 2018.
- [9] Aristotelis Chrysakis and Marie-Francine Moens. Online continual learning from imbalanced data. In *International Conference on Machine Learning*, pages 1952–1961. PMLR, 2020.
- [10] Trung-Anh Dang, Vincent Nguyen, Ngoc-Son Vu, and Christel Vrain. Memory-efficient continual learning with neural collapse contrastive. *arXiv preprint arXiv:2412.02865*, 2024.
- [11] Mehrdad Farajtabar, Navid Azizan, Alex Mott, and Ang Li. Orthogonal gradient descent for continual learning. In *International conference on artificial intelligence and statistics*, pages 3762–3773. PMLR, 2020.
- [12] Qiankun Gao, Chen Zhao, Bernard Ghanem, and Jian Zhang. R-dfcil: Relation-guided representation learning for data-free class incremental learning. In *European Conference on Computer Vision*, pages 423–439. Springer, 2022.
- [13] Spyros Gidaris and Nikos Komodakis. Dynamic few-shot visual learning without forgetting. In *Proceedings of the IEEE conference on computer vision and pattern recognition*, pages 4367–4375, 2018.
- [14] Kaiming He, Xiangyu Zhang, Shaoqing Ren, and Jian Sun. Deep residual learning for image recognition. In *Proceedings of the IEEE conference on computer vision and pattern recognition*, pages 770–778, 2016.
- [15] Saihui Hou, Xinyu Pan, Chen Change Loy, Zilei Wang, and Dahua Lin. Learning a unified classifier incrementally via rebalancing. In *2019 IEEE/CVF Conference on Computer Vision and Pattern Recognition (CVPR)*, pages 831–839. IEEE, 2019.
- [16] Ching-Yi Hung, Cheng-Hao Tu, Cheng-En Wu, Chien-Hung Chen, Yi-Ming Chan, and Chu-Song Chen. Compacting, picking and growing for unforgetting continual learning. *Advances in neural information processing systems*, 32, 2019.
- [17] James Kirkpatrick, Razvan Pascanu, Neil Rabinowitz, Joel Veness, Guillaume Desjardins, Andrei A Rusu, Kieran Milan, John Quan, Tiago Ramalho, Agnieszka Grabska-Barwinska, et al. Overcoming catastrophic forgetting in neural networks. *Proceedings of the national academy of sciences*, 114(13):3521–3526, 2017.

- [18] Alex Krizhevsky, Geoffrey Hinton, et al. Learning multiple layers of features from tiny images. 2009.
- [19] Yann Le, and Xuan Yang. Tiny imagenet visual recognition challenge. *CS 231N*, 7(7):3, 2015.
- [20] Sang-Woo Lee, Jin-Hwa Kim, Jaehyun Jun, Jung-Woo Ha, and Byoung-Tak Zhang. Overcoming catastrophic forgetting by incremental moment matching. *Advances in neural information processing systems*, 30, 2017.
- [21] Zhizhong Li and Derek Hoiem. Learning without forgetting. *IEEE transactions on pattern analysis and machine intelligence*, 40(12):2935–2947, 2017.
- [22] Sen Lin, Li Yang, Deliang Fan, and Junshan Zhang. Beyond not-forgetting: Continual learning with backward knowledge transfer. *Advances in Neural Information Processing Systems*, 35:16165–16177, 2022.
- [23] Sen Lin, Li Yang, Deliang Fan, and Junshan Zhang. Trgp: Trust region gradient projection for continual learning. *arXiv preprint arXiv:2202.02931*, 2022.
- [24] Hao Liu and Huaping Liu. Continual learning with recursive gradient optimization. *arXiv preprint arXiv:2201.12522*, 2022.
- [25] David Lopez-Paz and Marc’ Aurelio Ranzato. Gradient episodic memory for continual learning. *Advances in neural information processing systems*, 30, 2017.
- [26] Marc Masana, Xialei Liu, Bartłomiej Twardowski, Mikel Menta, Andrew D Bagdanov, and Joost Van De Weijer. Class-incremental learning: survey and performance evaluation on image classification. *IEEE Transactions on Pattern Analysis and Machine Intelligence*, 45(5):5513–5533, 2022.
- [27] Michael McCloskey and Neal J Cohen. Catastrophic interference in connectionist networks: The sequential learning problem. In *Psychology of learning and motivation*, volume 24, pages 109–165. Elsevier, 1989.
- [28] Mark D McDonnell, Dong Gong, Amin Parvaneh, Ehsan Abbasnejad, and Anton Van den Hengel. Ranpac: Random projections and pre-trained models for continual learning. *Advances in Neural Information Processing Systems*, 36:12022–12053, 2023.
- [29] Cuong V Nguyen, Yingzhen Li, Thang D Bui, and Richard E Turner. Variational continual learning. *arXiv preprint arXiv:1710.10628*, 2017.
- [30] Vardan Papayan, XY Han, and David L Donoho. Prevalence of neural collapse during the terminal phase of deep learning training. *Proceedings of the National Academy of Sciences*, 117(40):24652–24663, 2020.
- [31] Can Peng, Kun Zhao, Tianren Wang, Meng Li, and Brian C Lovell. Few-shot class-incremental learning from an open-set perspective. In *European Conference on Computer Vision*, pages 382–397. Springer, 2022.
- [32] Sylvestre-Alvise Rebuffi, Alexander Kolesnikov, Georg Sperl, and Christoph H Lampert. icarl: Incremental classifier and representation learning. In *Proceedings of the IEEE conference on Computer Vision and Pattern Recognition*, pages 2001–2010, 2017.
- [33] Matthew Riemer, Ignacio Cases, Robert Ajemian, Miao Liu, Irina Rish, Yuhai Tu, and Gerald Tesauero. Learning to learn without forgetting by maximizing transfer and minimizing interference. *arXiv preprint arXiv:1810.11910*, 2018.
- [34] Matthew Riemer, Ignacio Cases, Robert Ajemian, Miao Liu, Irina Rish, Yuhai Tu, and Gerald Tesauero. Learning to learn without forgetting by maximizing transfer and minimizing interference. In *International Conference on Learning Representations*. International Conference on Learning Representations, ICLR, 2019.
- [35] David Rolnick, Arun Ahuja, Jonathan Schwarz, Timothy Lillicrap, and Gregory Wayne. Experience replay for continual learning. *Advances in neural information processing systems*, 32, 2019.

- [36] Andrei A Rusu, Neil C Rabinowitz, Guillaume Desjardins, Hubert Soyer, James Kirkpatrick, Koray Kavukcuoglu, Razvan Pascanu, and Raia Hadsell. Progressive neural networks. *arXiv preprint arXiv:1606.04671*, 2016.
- [37] Gobinda Saha, Isha Garg, and Kaushik Roy. Gradient projection memory for continual learning. *arXiv preprint arXiv:2103.09762*, 2021.
- [38] Junao Shen, Qiyun Hu, Tian Feng, Xinyu Wang, Hui Cui, Sensen Wu, and Wei Zhang. In2nect: Inter-class and intra-class neural collapse tuning for semantic segmentation of imbalanced remote sensing images. In *Proceedings of the AAAI Conference on Artificial Intelligence*, volume 39, pages 6814–6822, 2025.
- [39] Hanul Shin, Jung Kwon Lee, Jaehong Kim, and Jiwon Kim. Continual learning with deep generative replay. *Advances in neural information processing systems*, 30, 2017.
- [40] James Seale Smith, Leonid Karlinsky, Vyshnavi Gutta, Paola Cascante-Bonilla, Donghyun Kim, Assaf Arbelle, Rameswar Panda, Rogerio Feris, and Zsolt Kira. Coda-prompt: Continual decomposed attention-based prompting for rehearsal-free continual learning. In *Proceedings of the IEEE/CVF conference on computer vision and pattern recognition*, pages 11909–11919, 2023.
- [41] Rishabh Tiwari, Krishnateja Killamsetty, Rishabh Iyer, and Pradeep Shenoy. Gcr: Gradient coresets based replay buffer selection for continual learning. In *Proceedings of the IEEE/CVF Conference on Computer Vision and Pattern Recognition*, pages 99–108, 2022.
- [42] Hao Wang, Yitong Wang, Zheng Zhou, Xing Ji, Dihong Gong, Jingchao Zhou, Zhifeng Li, and Wei Liu. Cosface: Large margin cosine loss for deep face recognition. In *Proceedings of the IEEE conference on computer vision and pattern recognition*, pages 5265–5274, 2018.
- [43] Liyuan Wang, Xingxing Zhang, Kuo Yang, Longhui Yu, Chongxuan Li, Lanqing Hong, Shifeng Zhang, Zhenguo Li, Yi Zhong, and Jun Zhu. Memory replay with data compression for continual learning. *arXiv preprint arXiv:2202.06592*, 2022.
- [44] Shipeng Wang, Xiaorong Li, Jian Sun, and Zongben Xu. Training networks in null space of feature covariance for continual learning. In *Proceedings of the IEEE/CVF conference on Computer Vision and Pattern Recognition*, pages 184–193, 2021.
- [45] Zifeng Wang, Zizhao Zhang, Sayna Ebrahimi, Ruoxi Sun, Han Zhang, Chen-Yu Lee, Xiaoqi Ren, Guolong Su, Vincent Perot, Jennifer Dy, et al. Dualprompt: Complementary prompting for rehearsal-free continual learning. In *European conference on computer vision*, pages 631–648. Springer, 2022.
- [46] Zifeng Wang, Zizhao Zhang, Chen-Yu Lee, Han Zhang, Ruoxi Sun, Xiaoqi Ren, Guolong Su, Vincent Perot, Jennifer Dy, and Tomas Pfister. Learning to prompt for continual learning. In *Proceedings of the IEEE/CVF conference on computer vision and pattern recognition*, pages 139–149, 2022.
- [47] Yichen Wen, Zhiqian Tan, Kaipeng Zheng, Chuanlong Xie, and Weiran Huang. Provable contrastive continual learning. In *Forty-first International Conference on Machine Learning*, 2019.
- [48] Robert Wu and Vardan Papyan. Linguistic collapse: Neural collapse in (large) language models. *Advances in Neural Information Processing Systems*, 37:137432–137473, 2024.
- [49] Liang Xie, Yibo Yang, Deng Cai, and Xiaofei He. Neural collapse inspired attraction–repulsion-balanced loss for imbalanced learning. *Neurocomputing*, 527:60–70, 2023.
- [50] Lu Xie, Weigang Li, and Yuntao Zhao. Hard example learning based on neural collapse for class-imbalanced semantic segmentation. *Applied Soft Computing*, page 112755, 2025.
- [51] Li Yang, Sen Lin, Junshan Zhang, and Deliang Fan. Grown: Grow only when necessary for continual learning. *arXiv preprint arXiv:2110.00908*, 2021.

- [52] Yibo Yang, Shixiang Chen, Xiangtai Li, Liang Xie, Zhouchen Lin, and Dacheng Tao. Inducing neural collapse in imbalanced learning: Do we really need a learnable classifier at the end of deep neural network? *Advances in neural information processing systems*, 35:37991–38002, 2022.
- [53] Yibo Yang, Haobo Yuan, Xiangtai Li, Zhouchen Lin, Philip Torr, and Dacheng Tao. Neural collapse inspired feature-classifier alignment for few-shot class incremental learning. *arXiv preprint arXiv:2302.03004*, 2023.
- [54] Yibo Yang, Haobo Yuan, Xiangtai Li, Jianlong Wu, Lefei Zhang, Zhouchen Lin, Philip Torr, Dacheng Tao, and Bernard Ghanem. Neural collapse terminus: A unified solution for class incremental learning and its variants. *arXiv preprint arXiv:2308.01746*, 2023.
- [55] Jaehong Yoon, Eunho Yang, Jeongtae Lee, and Sung Ju Hwang. Lifelong learning with dynamically expandable networks. *arXiv preprint arXiv:1708.01547*, 2017.
- [56] Friedemann Zenke, Ben Poole, and Surya Ganguli. Continual learning through synaptic intelligence. In *International conference on machine learning*, pages 3987–3995. PMLR, 2017.
- [57] Chen Zeno, Itay Golan, Elad Hoffer, and Daniel Soudry. Task-agnostic continual learning using online variational bayes with fixed-point updates. *Neural Computation*, 33(11):3139–3177, 2021.
- [58] Da-Wei Zhou, Zi-Wen Cai, Han-Jia Ye, De-Chuan Zhan, and Ziwei Liu. Revisiting class-incremental learning with pre-trained models: Generalizability and adaptivity are all you need. *International Journal of Computer Vision*, 133(3):1012–1032, 2025.
- [59] Didi Zhu, Zexi Li, Min Zhang, Junkun Yuan, Jiashuo Liu, Kun Kuang, and Chao Wu. Neural collapse anchored prompt tuning for generalizable vision-language models. In *Proceedings of the 30th ACM SIGKDD Conference on Knowledge Discovery and Data Mining*, pages 4631–4640, 2024.
- [60] Hui Zou, Trevor Hastie, and Robert Tibshirani. Sparse principal component analysis. *Journal of computational and graphical statistics*, 15(2):265–286, 2006.

A More Experimental Results

A.1 Experiment Details

A.1.1 Datasets

Seq CIFAR-10: Based on CIFAR-10 dataset [18], this benchmark partitions 10 classes into 5 sequential tasks (2 classes per task), and each class has 5000 and 1000 32×32 images each for training and testing, respectively;

Seq CIFAR-100: Constructed from CIFAR-100 [18], it comprises 10 tasks with 10 classes per task, and each class has 500 and 100 32×32 images each for training and testing, respectively;

Seq TinyImageNet: Adapted from the TinyImageNet dataset [19], this benchmark divides 200 classes into 10 sequential tasks (20 classes per task), and each class has 500 and 50 64×64 images each for training and testing, respectively.

A.1.2 Implementation Details

All experiments are conducted on a single RTX 4090 GPU. For all datasets, we employ a modified ResNet18 network architecture [14], where the kernel size of the first convolutional layer is modified from 7×7 to 3×3 , and the stride is changed from 2 to 1. The batch size is set to 32 across all experiments. The number of training epochs is set to 50 for Sequential CIFAR-10 and Sequential CIFAR-100, and 100 for Sequential TinyImageNet.

For ProNC, we consider the following hyperparameters: learning rate (η), weight of the alignment loss (λ_1), weight of the distillation loss (λ_2), momentum (mom), and weight decay (wd). The hyperparameters are selected through grid search. The chosen hyperparameters are presented in Table 5, and their corresponding search spaces are provided in Table 6.

Table 5: Hyperparameters of ProNC

Method	Buffer size	Dataset	Hyperparameter
Ours	200	Seq-CIFAR-10	η : 0.01, λ_1 : 13, λ_2 : 90, mom : 0, wd : 0
		Seq-CIFAR-100	η : 0.03, λ_1 : 18, λ_2 : 170, mom : 0, wd : 0
		Seq-Tiny-ImageNet	η : 0.03, λ_1 :20, λ_2 : 165, mom : 0, wd : 0
	500	Seq-CIFAR-10	η : 0.01, λ_1 :12, λ_2 : 80, mom : 0, wd : 0
		Seq-CIFAR-100	η : 0.03, λ_1 :18, λ_2 : 170, mom : 0, wd : 0
		Seq-Tiny-ImageNet	η : 0.03, λ_1 :20, λ_2 : 200, mom : 0, wd : 0

Table 6: Search Spaces for Hyperparameters

Hyperparameter	Values
η	{0.01, 0.03, 0.05, 0.1, 0.3}
λ_1	{5, 10, 12, 13, 18, 20}
λ_2	{50, 75, 80, 90, 165, 170, 200}
mom	{0, 0.9}
wd	{0, 10^{-5} , 5×10^{-5} }

Our code is implemented based on the Continual Learning platform Mammoth [4], which is also provided in the supplementary materials.

A.2 More Results

A.2.1 Final Average Accuracy with Error Bars

Table 7: Final average accuracies comparison under various setups. All results are averaged over multiple runs.

Buffer	Method	Seq-Cifar-10		Seq-Cifar-100		Seq-Tiny-ImageNet	
		Class-IL	Task-IL	Class-IL	Task-IL	Class-IL	Task-IL
200	ER [34]	44.79 \pm 1.86	91.19 \pm 0.94	21.78 \pm 0.48	60.19 \pm 1.01	8.49 \pm 0.16	38.17 \pm 2.00
	iCaRL [32]	49.02 \pm 3.20	88.99 \pm 2.13	28 \pm 0.91	51.43 \pm 1.47	7.53 \pm 0.79	28.19 \pm 1.47
	GEM [25]	25.54 \pm 0.76	90.44 \pm 0.94	20.75 \pm 0.66	58.84 \pm 1.00	—	—
	GSS [2]	39.07 \pm 5.59	88.8 \pm 2.89	19.42 \pm 0.29	55.38 \pm 1.34	—	—
	DER [5]	61.93 \pm 1.79	91.4 \pm 0.92	31.23 \pm 1.38	63.09 \pm 1.09	11.87 \pm 0.78	40.22 \pm 0.67
	DER++ [5]	64.88 \pm 1.17	91.92 \pm 0.60	28.13 \pm 0.51	66.80 \pm 0.41	11.34 \pm 1.17	43.06 \pm 1.16
	Co ² L [6]	51.27 \pm 1.86	84.69 \pm 1.52	18.09 \pm 0.49	49.19 \pm 0.91	12.95 \pm 0.06	37.07 \pm 1.62
	CILA [47]	59.68 \pm 0.65	91.36 \pm 0.08	19.49 \pm 0.53	53.93 \pm 1.02	12.98 \pm 0.10	37.32 \pm 1.87
	MNC ³ L [10]	52.20 \pm 1.56	85.94 \pm 0.22	15.81 \pm 0.48	43.91 \pm 0.76	10.57 \pm 1.66	32.78 \pm 3.54
	NCT [54]	51.59 \pm 0.41	80.63 \pm 0.46	26.38 \pm 0.57	75.75 \pm 0.17	10.95 \pm 1.45	52.71 \pm 4.12
	Ours	65.58 \pm 0.15	96.86 \pm 0.10	42.99 \pm 0.85	85.63 \pm 0.73	27.44 \pm 1.00	69.09 \pm 0.65
500	ER [34]	57.74 \pm 2.48	93.61 \pm 0.27	27.66 \pm 0.61	66.23 \pm 1.52	9.99 \pm 0.29	48.64 \pm 0.46
	iCaRL [32]	47.55 \pm 3.95	88.22 \pm 2.62	33.25 \pm 1.25	58.16 \pm 1.76	9.38 \pm 1.53	31.55 \pm 3.27
	GEM [25]	26.2 \pm 1.26	92.16 \pm 0.64	25.54 \pm 0.65	66.31 \pm 0.86	—	—
	GSS [2]	49.73 \pm 4.78	91.02 \pm 1.57	21.92 \pm 0.34	60.28 \pm 1.18	—	—
	DER [5]	70.51 \pm 1.67	93.40 \pm 0.21	41.36 \pm 1.76	71.73 \pm 0.74	17.75 \pm 1.14	51.78 \pm 0.88
	DER++ [5]	72.70 \pm 1.36	93.88 \pm 0.50	38.20 \pm 1.00	74.77 \pm 0.31	19.38 \pm 1.41	51.91 \pm 0.68
	Co ² L [6]	61.78 \pm 4.22	89.51 \pm 2.45	26.64 \pm 1.42	62.32 \pm 0.19	18.71 \pm 0.84	50.74 \pm 1.24
	CILA [47]	67.82 \pm 0.33	93.29 \pm 0.24	31.27 \pm 0.17	68.29 \pm 0.46	18.09 \pm 0.49	49.19 \pm 0.91
	MNC ³ L [10]	52.20 \pm 1.56	85.94 \pm 0.22	22.29 \pm 0.18	56.43 \pm 0.29	11.52 \pm 0.01	36.32 \pm 0.05
	NCT [54]	60.93 \pm 0.94	81.27 \pm 0.24	33.84 \pm 0.38	76.06 \pm 0.52	18.24 \pm 0.62	62.30 \pm 0.41
	Ours	73.95 \pm 0.68	96.95 \pm 0.14	48.94 \pm 0.44	86.38 \pm 0.43	29.06 \pm 0.32	69.77 \pm 0.89

A.3 Final Forgetting with Error Bars

Table 8: Final forgetting comparison under various setups. All results are averaged over multiple runs.

Buffer	Method	Seq-Cifar-10		Seq-Cifar-100		Seq-Tiny-ImageNet	
		Class-IL	Task-IL	Class-IL	Task-IL	Class-IL	Task-IL
200	ER [34]	59.30 \pm 2.48	6.07 \pm 1.09	75.06 \pm 0.63	27.38 \pm 1.46	76.53 \pm 0.51	40.47 \pm 1.54
	iCaRL [32]	23.52 \pm 1.27	25.34 \pm 1.64	47.20 \pm 1.23	36.20 \pm 1.85	31.06 \pm 1.91	42.47 \pm 2.47
	GEM [25]	80.36 \pm 5.25	9.57 \pm 2.05	77.40 \pm 1.09	29.59 \pm 1.66	—	—
	GSS [2]	72.48 \pm 4.45	8.49 \pm 2.05	77.62 \pm 0.76	32.81 \pm 1.75	—	—
	DER [5]	35.79 \pm 2.59	6.08 \pm 0.70	62.72 \pm 2.69	25.98 \pm 1.55	64.83 \pm 1.48	40.43 \pm 1.05
	DER++ [5]	32.59 \pm 2.32	5.16 \pm 0.21	60.99 \pm 1.52	23.91 \pm 0.55	73.47 \pm 1.23	39.02 \pm 0.43
	Co ² L [6]	30.17 \pm 8.57	2.91 \pm 5.25	64.14 \pm 0.69	36.81 \pm 0.63	62.04 \pm 0.28	40.75 \pm 3.55
	CILA [47]	37.52 \pm 5.84	5.49 \pm 0.74	64.01 \pm 0.18	33.07 \pm 0.96	63.11 \pm 0.61	41.40 \pm 0.51
	MNC ³ L [10]	33.74 \pm 1.65	4.90 \pm 0.15	62.51 \pm 0.40	39.79 \pm 0.98	59.68 \pm 2.02	45.10 \pm 1.57
	NCT [54]	22.48 \pm 19.50	1.41 \pm 1.09	27.40 \pm 1.65	4.79 \pm 0.07	49.33 \pm 4.47	15.88 \pm 0.95
	Ours	32.75 \pm 4.71	0.65 \pm 0.08	36.07 \pm 0.51	4.40 \pm 0.82	42.81 \pm 0.56	9.42 \pm 0.58
500	ER [34]	43.22 \pm 2.10	3.50 \pm 0.53	67.96 \pm 0.78	17.37 \pm 1.06	75.21 \pm 0.54	30.73 \pm 0.62
	iCaRL [32]	28.20 \pm 2.41	22.61 \pm 3.97	40.99 \pm 1.02	27.90 \pm 1.37	37.30 \pm 1.42	39.44 \pm 0.84
	GEM [25]	78.93 \pm 6.53	5.60 \pm 0.96	71.34 \pm 0.78	20.44 \pm 1.13	—	—
	GSS [2]	59.18 \pm 4.00	6.37 \pm 1.55	74.12 \pm 0.42	26.57 \pm 1.34	—	—
	DER [5]	24.02 \pm 1.63	3.72 \pm 0.55	49.07 \pm 2.54	25.98 \pm 1.55	59.95 \pm 2.31	28.21 \pm 0.97
	DER++ [5]	22.38 \pm 4.41	4.66 \pm 1.15	49.18 \pm 2.19	15.75 \pm 0.48	58.75 \pm 1.93	25.47 \pm 1.03
	Co ² L [6]	17.79 \pm 3.36	2.65 \pm 1.00	48.60 \pm 1.34	23.47 \pm 0.27	49.64 \pm 1.14	13.80 \pm 2.10
	CILA [47]	18.22 \pm 1.32	0.65 \pm 0.13	45.67 \pm 1.02	16.98 \pm 0.56	64.14 \pm 0.69	27.83 \pm 1.32
	MNC ³ L [10]	27.88 \pm 2.75	3.15 \pm 0.42	46.09 \pm 0.58	24.29 \pm 0.50	44.96 \pm 0.09	39.00 \pm 0.17
	NCT [54]	13.82 \pm 3.64	3.84 \pm 0.35	24.37 \pm 5.42	3.97 \pm 0.75	50.90 \pm 1.16	6.84 \pm 0.87
	Ours	26.75 \pm 1.29	0.24 \pm 0.14	24.32 \pm 0.24	4.35 \pm 0.17	38.58 \pm 0.39	9.52 \pm 0.96

A.4 Generality and Flexibility of Our Designs

As discussed in Section 5.2, our approach introduces a novel and effective feature regularization method based on ProNC, which can be generally incorporated into different CL frameworks. To further verify this, we conduct more experiments by plugging ProNC into established replay-based methods (iCaRL [32] and LUCIR [15]) with the alignment loss as an additional regularization term

in their objective functions. In particular, we keep all the components the same as the original designs in these studies (including the classifier design) and only incorporate ProNC with the alignment loss.

Table 9 shows the performance comparison between the original implementations of iCaRL and LUCIR and the versions enhanced with ProNC-based regularization. The experiments are conducted under the Class-IL setting on Seq-CIFAR-100 with a memory buffer size of 500. It can be seen that incorporating the ProNC regularization yields substantial performance improvements, i.e., 16.90% over iCaRL and 8.28% over LUCIR, which clearly demonstrates the potential and generality of ProNC as a feature regularization for CL.

Table 9: Impact of ProNC regularization term

Methods	FAA
iCaRL [32]	33.25
iCaRL with ProNC	38.87
LUCIR [15]	37.68
LUCIR with ProNC	40.80

Table 10: Impact of different loss design

Loss Combination	FAA
$\mathcal{L}_{\text{align}} + \mathcal{L}_{\text{distill}}$	48.94
$\mathcal{L}_{\text{align}} + l_2\text{-Norm loss}$	49.42
$l_2\text{-Norm loss} + \mathcal{L}_{\text{distill}}$	48.61
$l_2\text{-Norm loss} + l_2\text{-Norm loss}$	48.66

Moreover, our approach is also very flexible in the sense that the loss terms in the final objective function can be replaced by other designs. To show this, we replace the cosine-similarity in the loss functions, i.e., $\mathcal{L}_{\text{align}}$ and $\mathcal{L}_{\text{distill}}$, by using a standard l_2 -norm, and conduct experiments under the Class-IL setting on Seq-CIFAR-100 with a memory buffer size of 500. As shown in Table 10, the performance of our approach is stable under different design combinations when we replace the cosine similarity in any of the two loss terms, which further corroborate the flexibility of our approach. In principle, our approach can be generally applied with a loss function that seeks to minimize the distance between the learned features and the ETF target/old features.

B Proof of Theorem 1

Based on the definition of ETF, we know that \mathbf{E}^* can be expressed as

$$\mathbf{E}^* = \sqrt{\frac{K_1}{K_1 - 1}} \mathbf{U}^* \left(\mathbf{I}_{K_1} - \frac{1}{K_1} \mathbf{1}_{K_1} \mathbf{1}_{K_1}^\top \right), \quad (7)$$

where $\mathbf{U}^* \in \mathbb{R}^{d \times K_1}$ denotes the corresponding orthogonal matrix.

Because $\mathbf{U}' = \sqrt{\frac{K_1 - 1}{K_1}} \tilde{\mathbf{M}}_{K_1} \left(\mathbf{I}_{K_1} - \frac{1}{K_1} \mathbf{1}_{K_1} \mathbf{1}_{K_1}^\top \right)$, we can have

$$\tilde{\mathbf{M}} = \sqrt{\frac{K_1}{K_1 - 1}} \mathbf{U}' \left(\mathbf{I}_{K_1} - \frac{1}{K_1} \mathbf{1}_{K_1} \mathbf{1}_{K_1}^\top \right). \quad (8)$$

This is true since $\mathbf{I}_{K_1} - \frac{1}{K_1} \mathbf{1}_{K_1} \mathbf{1}_{K_1}^\top$ is an orthogonal projection matrix with rank $K_1 - 1$ and also equal to its pseudoinverse.

It is clear that

$$\begin{aligned} \tilde{\mathbf{M}}_{K_1} - \mathbf{E}^* &= \sqrt{\frac{K_1}{K_1 - 1}} \mathbf{U}' \left(\mathbf{I}_{K_1} - \frac{1}{K_1} \mathbf{1}_{K_1} \mathbf{1}_{K_1}^\top \right) - \sqrt{\frac{K_1}{K_1 - 1}} \mathbf{U}^* \left(\mathbf{I}_{K_1} - \frac{1}{K_1} \mathbf{1}_{K_1} \mathbf{1}_{K_1}^\top \right) \\ &= \sqrt{\frac{K_1}{K_1 - 1}} (\mathbf{U}' - \mathbf{U}^*) \left(\mathbf{I}_{K_1} - \frac{1}{K_1} \mathbf{1}_{K_1} \mathbf{1}_{K_1}^\top \right). \end{aligned}$$

Since $\sqrt{\frac{K_1}{K_1 - 1}}$ is a scalar and $\mathbf{I}_{K_1} - \frac{1}{K_1} \mathbf{1}_{K_1} \mathbf{1}_{K_1}^\top$ is a fixed projection matrix, finding \mathbf{E}^* to minimize $\|\tilde{\mathbf{M}}_{K_1} - \mathbf{E}^*\|_F^2$ is equivalent to finding an orthogonal matrix \mathbf{U}^* that minimizes $\|\mathbf{U}' - \mathbf{U}^*\|_F^2$.

To this end, the following lemma [60] characterizes the nearest orthogonal matrix to any real matrix.

Lemma 1 (Nearest Orthogonal Matrix via SVD). *Let $\mathbf{A} \in \mathbb{R}^{m \times n}$ be a real matrix with Singular Value Decomposition (SVD) $\mathbf{A} = \mathbf{W} \mathbf{\Sigma} \mathbf{V}^\top$, where $\mathbf{W} \in \mathbb{R}^{m \times s}$ and $\mathbf{V} \in \mathbb{R}^{s \times n}$ are orthogonal matrices, and $\mathbf{\Sigma} \in \mathbb{R}^{s \times s}$ is a diagonal matrix of singular values with $s = \min(m, n)$. The nearest orthogonal matrix $\mathbf{Q} \in \mathbb{R}^{m \times n}$ to \mathbf{A} under Frobenius norm is:*

$$\mathbf{Q} = \mathbf{W} \mathbf{V}^\top.$$

Therefore, given the SVD of \mathbf{U}' as $\mathbf{W}\mathbf{\Sigma}\mathbf{V}^\top$, the orthogonal matrix closest to \mathbf{U}' can be represented as $\mathbf{U}^* = \mathbf{W}\mathbf{V}^\top$, which will lead to an ETF matrix

$$\mathbf{E}^* = \sqrt{\frac{K_1}{K_1 - 1}} \mathbf{W}\mathbf{V}^\top \left(\mathbf{I}_{K_1} - \frac{1}{K_1} \mathbf{1}_{K_1} \mathbf{1}_{K_1}^\top \right).$$